La radiologia medica (2019) 124:1238–1252
https://doi.org/10.1007/s11547-019-01097-7

CARDIAC RADIOLOGY

Third-generation dual-source dual-energy CT in pediatric congenital heart disease patients: state-of-the-art

Nicolò Schicchi[1] · Marco Fogante[1] · Paolo Esposto Pirani[1] · Giacomo Agliata[1] · Maria Chiara Basile[1] · Matteo Oliva[1] · Andrea Agostini[1] · Andrea Giovagnoni[1]

Received: 23 September 2019 / Accepted: 9 October 2019 / Published online: 19 October 2019

Abstract
Cardiovascular computer tomography (CT) in pediatric congenital heart disease (CHD) patients is often challenging. This might be due to limited patient cooperation, the high heart rate, the complexity and variety of diseases and the need for radiation dose minimization. The recent developments in CT technology with the introduction of the third-generation dual-source (DS) dual-energy (DE) CT scanners well suited to respond to these challenges. DSCT is characterized by high-pitch, long anatomic coverage and a more flexible electrocardiogram-synchronized scan. DE provides additional clinical information about vascular structures, myocardial and lung perfusion and allows artifacts reduction. These advances have increased clinical indications and modified CT protocol for pediatric CHD patients. In our hospital, DSCT with DE technology has rapidly become an important imaging technique for both pre- and postoperative management of pediatric patients with CHDs. The aim of this article is to describe the state-of-the-art in DSCT protocol with DE technology in pediatric CHD patients, providing some case examples of our experience over an 18-month period.

Keywords Dual-source CT · Dual-energy CT · Congenital heart disease · Pediatric patients · State-of-the-art

Introduction

Congenital heart disease (CHD) is the most common inborn pathology with an incidence of 1% and a prevalence of 8–10 per 1000 live births. Radiological assessment is based on the clinical distinction in acyanotic or cyanotic CHD [1]. Table 1 shows the main CHDs.

Imaging assessment of pediatric CHD patients is challenging for the wide spectrum of disease and complex congenital defects, high heart rates, motion artifacts from cardiac and respiration movements and limited patient cooperation. Therefore, short examination time and high temporal and spatial resolution are required. Imaging modalities for evaluating CHD in pediatric patients include echocardiography, conventional invasive angiography, magnetic resonance imaging (MRI) and computed tomography (CT) [2, 3]. CT is an excellent modality, given the rapid acquisition times and the comprehensive and the accurate three-dimensional evaluation of complex anatomy [4]. Despite these advantages, the high heart rate, the use of ionizing radiation and the limited patient cooperation are limiting factors and CT is not the modality of choice for imaging in pediatric patients [5]. However, the development in CT technology with the introduction of the third-generation dual-source (DS) dual-energy (DE) CT scanners well suited to respond to these challenges [6].

The aim of this article is to describe the state-of-the-art in DSCT protocol with DE technology in pediatric CHD patients to obtain high-quality images with low radiation dose, providing some case examples of our experience over an 18-month period.

Technical parameters

Third-generation DSCT scanner uses two X-ray tubes working at the same energy (single-energy) or at different energy (DE). Two X-ray tubes are placed approximately at 95° to each other and can work at high (from 120 to

✉ Marco Fogante
marco.fogante89@gmail.com

[1] Radiology Department, Azienda Ospedaliero Universitaria "Ospedali Riuniti", 60126 Ancona, Italy

Table 1 Clinical classification of congenital heart diseases

Acyanotic heart disease
Increased pulmonary venous flow (pulmonary edema)
Hypoplastic left heart
Aortic coarctation
Interrupted aortic arch
Congestive heart failure
Neonatal sepsis
Increased pulmonary arterial flow (shunt vascularity)
Atrial septal defect
Ventricular septal defect
Patent ductus arteriosus
Atrio-ventricular canal defect
Cyanotic heart disease
Decreased pulmonary vascularity with cardiomegaly
Ebstein anomaly
Decreased pulmonary vascularity without cardiomegaly
Tetralogy of Fallot
Usually increased pulmonary vascularity without cardiomegaly
Transposition of great arteries
Truncus arteriosus
Tricuspid atresia
Partial/total anomalous pulmonary venous return
Single ventricle

150 kV) and at low (from 70 to 100 kV) energies [7–9]. Third-generation DS systems have a tin filter in front of the high-energy tube, that attenuates lower energy photons, thereby increasing the difference of spectral energy. Tin filter provides the separation of the low- and high-energy spectra and improves the capacity of differentiation between clinically relevant materials, such as calcium and iodine. The fastest gantry rotation speed is 250 ms, allowing the almost simultaneous acquisition of the two energy spectra. The highest pitch value is 3.2. The highest temporal resolution is 66 ms [10–12]. A limitation of the DS scanner is the field of view (FOV). The FOV of the low-energy tube is 50 cm, whereas the FOV of the high-energy tube is 35 cm. The potential disadvantage of the FOV of the smaller tube is the evaluation of the structures located peripherally in larger patient. However, in pediatric patients, this is not a problem [13, 14]. Each cardiac CT examination should be tailored to increase diagnostic information and reduce radiation dose. Third-generation DS-DECT allows a submillimeter spatial resolution of the heart and coronary arteries in one or a few heartbeats, a high temporal resolution, a radiation dose reduction with high-pitch values and low tube voltage, new algorithms of iterative reconstruction, and provides additional clinical information with DE technology. Table 2 summarizes technical parameters of the third-generation DS-DECT scanner [15, 16].

Table 2 Technical parameters of third-generation dual-source dual-energy CT scanner

Technical parameters	Third-generation dual-source dual-energy CT
Number of detector	384 (192×2)
Detector *z*-dimension	0.6 mm
Rotation time	0.25 s
Temporal resolution	66 ms
Spatial resolution	0.24 mm
z-axis coverage	115.2 (57.6×2) mm
Maximum scan speed	737 mm/s
Field of view—main tube	50 cm
Field of view—secondary tube	35 cm

Patient preparation

Pediatric patients should be positioned in supine position, with the arms above the head, at the isocenter of the CT scanner. The electrodes should be located outside the thoracic region, on the arms and upper abdomen, to prevent image-quality reduction or radiation dose increase. Third-generation DSCT makes possible to scan non-cooperative pediatric patients with minimal sedation, free breathing and without β-blockage of heart rate, even to heart rate around 140 beats/min. The highest temporal resolution should be used to minimize motion artifacts. However, minimal sedation in restless patients can be considered [17, 18]. Breathing artifacts can be quite tricky and are often seen in single-source CT, but hardly in DSCT [19]. However, when distal or detailed coronary artery imaging is needed, breath-holding is beneficial. If children are compliant, practicing the breath-hold before the examination helps to maximize cooperation and assess respiratory sinus arrhythmia. Otherwise, anesthesia with suspended respiration can be considered [20]. Beta-blockers are often not needed to given that they prolong patient preparation time with no guaranteed success. Nevertheless, beta-blockers are safe in pediatric patients without contraindications and should be considered if high-definition imaging is required because image quality remains heart-pulse-dependent [21].

Contrast injection

Third-generation DSCT allows contrast volume saving, because using a low tube voltage (70 kV) X-rays generated have an average energy close to the k-edge of iodine (33.2 keV), improving contrast enhancement. Moreover, the fast scan protocol provides precise shaping and timing

of the contrast peak enhancement for optimal intravascular attenuation and allows reducing contrast volume [22]. For these reasons, keeping the iodine delivery rate constant, contrast medium (CM) with low iodine concentration (300 mgI/ml) showed a higher vascular enhancement than CM with high iodine concentration (400 mgI/ml), allowing iodine load reduction. CM is usually injected through a peripheral vein using a dual-syringe power injector. Intravenous line size ranging from 24-gauge in neonates to 18-gauce in older children, with flow rates between 0.5 and 5 ml/s and pressure settings of 50–300 lb per square inch (psi). Central venous catheter might be used in critically pediatric patient, but it allows for adequate injection in children with age less than 1-year because maximum flow rate is 0.4–1.2 ml/s and maximum pressure value is 25–50 psi. Contrast concentration should be 300–400 mgI/ml, considering the intravenous access and body weight. A dose of 1.0–1.5 ml/kg of CM is normally necessary. With gated evaluation, the dose can be smaller (0.5–1.0 ml/kg). A larger dose up to 2.0 ml/kg is necessary with large intra-cardiac or extra-cardiac shunts, valve regurgitations and a severe cardiomegaly. If a second CT acquisition is necessary, an additional contrast dose of 1.0–1.5 ml/kg should be administered. Anyhow, the maximal dosage should be 3.0 ml/kg [23]. Special care must be taken to avoid accidental injection of air, which can result in paradoxical embolism in the presence of intra-cardiac shunting. The most common injection protocols include a biphasic or triphasic approach. The biphasic approach entails a contrast bolus followed by a saline flush with slower flow rate. This approach should be used for coronary artery evaluation in pediatric patients without cardiovascular lesions. The triphasic approach consists of a two-phase contrast administration (about half at the regular rate plus the remainder either at a slower rate) followed by saline with slower flow rate. This method should be used for the assessment of complex cardiovascular disease to obtain simultaneous evaluation of right and left-side structures [24, 25].

Scan timing

Scan time can be decided with three different techniques: fixed-time, bolus-test and bolus-tracking. Fixed-time technique consists of initiating the scan at the end of the injection. The site of cannulation and scan protocol must be considered; an extra delay of 2–4 s should be added when injecting from the leg and when using shorter scan methods. This approach avoids unnecessary radiation exposure related to the use of bolus monitoring and might be best suited for infants and younger children. Nevertheless, this technique is prone to inaccuracy and it is challenging because it is limited reproducibility from the different time of contrast transit for anatomical, functional and technical reasons [26].

Bolus-test technique consists of calculating vascular peak enhancement time of a small contrast volume by monitoring CM transit on a selected slice. An extra delay, usually 3–6 s, should be added in the scan acquisition depending on protocols, 3 s using retrospective protocol and 6 s using prospective protocol. This method involves additional CM and radiation and it is not routinely applicate in children [27].

Bolus-tracking technique is the most useful in pediatric patients. Automatic or visual approach is usually used to decide the scan starting. Compared to bolus-test, bolus-tracking allows homogeneous enhancement with less contrast volume. The region of interest should be placed within the ascending aorta and the trigger threshold should be set at 100 HU. When is necessary the visualization of the cardiac chambers and the descending aorta in the same plane, the region of interest could be placed within the left ventricle and the trigger threshold should be set 100 HU. Automatic start should be used with cooperative patients. Visual start should be used with restless patients because with automatic approach, the movements of the patient during the bolus measurement can cause to start too early or too late. Moreover, it is recommended to switch from the automatic to the visual start when threshold enhancement is not reached. To reduce radiation exposure, monitoring should start at the end of contrast injection and should be reduced in frequency (one each second), and tube voltage should be reduced (70 kV) [28].

Scan protocol

The scan range should include the heart, the thoracic aorta and the pulmonary arteries.

The scan acquisition can be non-electrocardiogram (ECG)-synchronized or ECG-synchronized.

Non-ECG-synchronized acquisition

Non-ECG-synchronized acquisition should be used when the diagnostic purpose concerns extra-cardiac anatomy. The high temporal resolution allows for good quality imaging of extra-cardiac structures because they are less sensitive to heart motion than the heart itself [29]. Moreover, respiratory artifacts are responsible for imaging degradation and non-synchronized acquisition is obtained more quickly than synchronized acquisition, and thus is responsible for fewer respiratory artifacts [30]. Finally, synchronized acquisition requires a much higher radiation dose than non-synchronized acquisition because the exposure time is longer due to low pitch acquisitions [31].

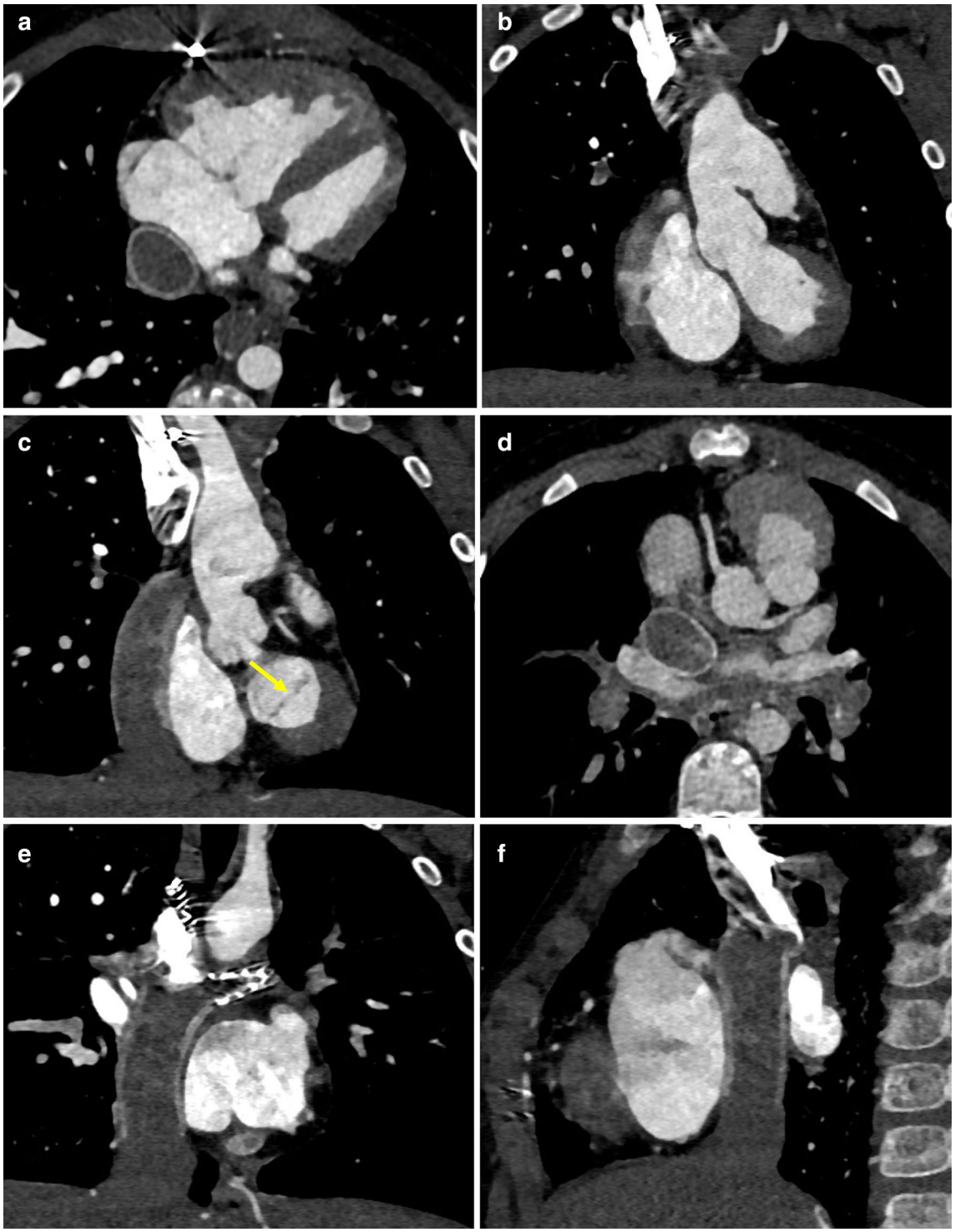

Fig. 1 DSCT images in a 3-year-old patient with hypoplastic left heart syndrome treated with modified Fontan procedure. Hypoplastic left ventricle with high wall thickness, in axial (**a**) and coronal (**b**) views. Mitral valve partially closed (**c**) (yellow arrow). Coronary arteries origin from aortic valve (**d**) (yellow arrows). Modified Fontan procedure, a lateral tunnel created near the right atrium to direct blood from the inferior vena cava to the right pulmonary artery and a stent into the left pulmonary artery, in coronal (**e**) and sagittal (**f**) views

Table 3 DSCT protocol in a 3-year-old patient with hypoplastic left heart syndrome treated with modified Fontan procedure

Scan parameters	
Tube voltage	70 kV
Tube current	30–60 mAs
Pitch factor	3.2
Collimation	2 × 196 × 0.6 mm
Rotation time	0.25 s
Scan protocol	Prospective ECG-triggered high pitch
Reconstruction parameters	
Slice width	0.6 mm
Slice increment	0.4 mm
Kernel–strength	Bv40–3
Cardiac phase	30%
Radiation dose	
CTDI	0.8 mGy
DLP	51.2 mGy * cm
SSDE	1.2 mGy
Effective dose	1.0 mSv
Contrast medium	
Concentration	320 mgI/ml
Dose	1 ml/kg
Volume	18 ml

DSCT, electrocardiogram; Bv, Body vascular; $CTDI_{vol}$, volume computed tomography dose index; DLP, dose length product; SSDE, size-specific dose estimates

ECG-synchronized acquisition

ECG-synchronized acquisition should be used when the diagnostic purpose concerns intra-cardiac anatomy. To prevent a radiation dose increase the automatic ECG radiation modulation should be use [32]. The ECG radiation modulation avoids large increase in radiation dose even with irregular heart rate. It is recommended to keep a wider acquisition and radiation margin, allowing flexibility in reconstruction window to minimize motion. The main acquisition modes include: prospective ECG-triggered high-pitch spiral, prospective ECG-gated sequential, and retrospective ECG-gated spiral [33].

Prospective ECG-triggered high-pitch spiral mode should be used in uncooperative patients because it reduces respiratory and cardiac motion artifacts, as well as the need for sedation and general anesthesia. This mode uses two X-ray tubes to achieve both maximum temporal resolution and *z*-axis scan speed, resulting in rapid and large gapless non-overlapping imaging in a single heartbeat. The length of the R–R interval in pediatric patients is around 500 ms at a heart rate of around 120 beats/min. An ECG-triggered high-pitch scan with a 12 cm scan length takes up to 130 ms. With increasing heart rate, the mean velocity of all coronary arteries significantly increases. ECG-synchronized high pitch should be triggered with the diastolic phase to avoid cardiac motion artifacts. Sometimes, motion coronary artifacts can be occurred due to the high heart rate and relative short motion free acquisition time. Mostly, only information on the anatomy is required and not the rule out of coronary artery disease as in adults, providing sufficient diagnostic image quality [34].

Prospective ECG-gated sequential mode should be used in cooperative patients with irregular heart rate. This mode allows to increase the percentage of the cardiac cycle phase acquired (from 30 to 60% of the diastolic phase), to select the ECG phase without motion artifacts, and avoid non-diagnostic scans [35]. An issue of prospective ECG-gated sequential mode is the possibility of a stack artifact when scanning a larger length in the *z*-axis than the collimation width. In children, because the length of the *z*-axis is not elevated and the focus is mainly on anatomy assessment, the stack artifacts can be less problematic [36].

Retrospective ECG-gated spiral mode should be use with very irregular heart rate where the need for ECG editing is expected, or when the functional cardiac information could be necessary. This mode allows acquiring the entire cardiac cycle, selecting the heart phase without motion artifacts and evaluating functional cardiac parameters. An issue of retrospective ECG-gated spiral mode is the increase in the radiation exposure. Lower radiation dose is feasible with the use of pulsing techniques. This technique loses efficiency at higher heart rate because of less efficient slope-up time and slope-down time of the ECG-based tube current modulation [37].

DE clinical applications

DE clinical applications in pediatric CHD patients include better evaluation of vascular structures and shunts, assessment of the myocardial and lung perfusion and reduction in metal artifact. The two X-ray tubes operate independently at low (70–80 kV) and high (140–150 kV) energies. With DE technology is necessary the use of the retrospective ECG-gated spiral scanning mode. The post-processing techniques that best exploit the advantages of DE in CHDs are "material decomposition" and "virtual mono-energetic" [38].

"Material decomposition" allows discriminating structures based on attenuation characteristics at different energy levels. The system uses "three-material decomposition" algorithm in the image-space domain. The three materials used for material differentiation in pediatric CHD are soft tissue, calcium, and iodine. One application profile is the automatic bone removal, which separates iodine from bone. In the reconstructed image, iodinated vessels are the only remaining dense material, improving evaluation of vasculature. This application reduces significantly errors in bone

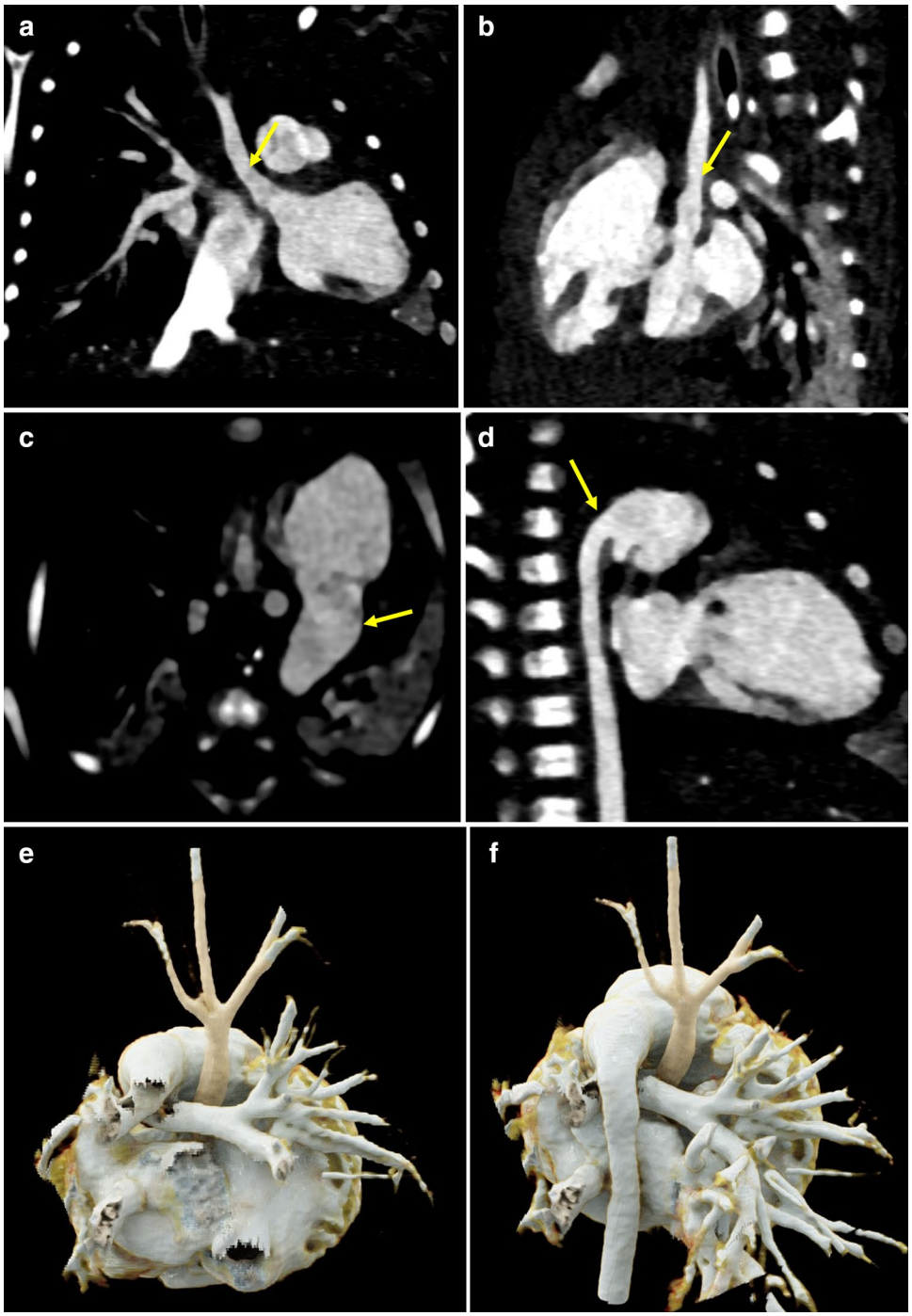

Fig. 2 DSCT images in a 12-day-old patient with IAA and PDA. Type A interrupted aortic arch, after the left subclavian artery origin, with a gap between the ascending and descending thoracic aorta, in sagittal (**a**) and coronal (**b**) views (yellow arrows). Patent ductus arteriosus with the descending aorta continuation of the ductus (**c**, **d**) (yellow arrows). Volume rendering reconstructions in superior (**e**) and posterior (**f**) views

segmentation compared with the threshold attenuation, based single-energy technique. Another application is the virtual non-contrast, which allows obtaining virtual non-enhanced images and iodine overlay images [39]. Virtual non-enhanced images could obviate a true non-enhanced acquisition, reducing radiation dose. Iodine overlay images allow quantitative evaluation of iodine content, a reference region is placed in an area of maximum contrast enhancement and another region of interest in placed in the target area of a contrast material–enhanced image. Because absolute threshold values for increased or decreased iodine content have not been defined and iodine measurements may vary among vendors, the quantitative analysis is best performed by assessing relative contrast enhancement values [40]. Another application is the evaluation of myocardial perfusion, which provides the myocardial iodine distribution during the first pass arterial enhancement and can detect myocardial blood supply [41]. Finally, the lung analysis

Table 4 DSCT protocol in a 12-day-old patient with IAA and PDA

Scan parameters	
Tube voltage	70 kV
Tube current	30–60 mAs
Pitch factor	3.2
Collimation	2 × 196 × 0.6 mm
Rotation time	0.25 s
Scan protocol	Prospective ECG-triggered high pitch
Reconstruction parameters	
Slice width	0.6 mm
Slice increment	0.4 mm
Kernel–strength	Bv40–3
Cardiac phase	30%
Radiation dose	
CTDI	0.2 mGy
DLP	13.4 mGy * cm
SSDE	0.3 mGy
Effective dose	0.9 mSv
Contrast medium	
Concentration	320 mgI/ml
Dose	0.5 ml/kg
Volume	2 ml

DSCT, electrocardiogram; Bv, Body vascular; $CTDI_{vol}$, volume computed tomography dose index; DLP, dose length product; SSDE, size-specific dose estimates

application allows assessing qualitative and quantitative lung perfusion. DECT may be an efficient method to assess perfused lung blood volume in CHDs, such as pulmonary atresia, arteriovenous malformations and tetralogy of Fallot [42]. DECT allows simultaneous evaluation of lung vessels and parenchyma without extra-radiation in a single acquisition. The perfused blood volume image shows homogenous iodine distribution in the lung parenchyma. Normal pulmonary blood flow is typically gravity-related. Areas with perfusion defect appear with decreased or absent iodine content. These perfusion defects correlate with increased right-to-left shunt and combined with the morphologic analysis can improve detectability of the cyanotic CHD [43].

"Virtual mono-energetic" allows reconstruction of virtual images that simulate the attenuation values of an image acquired by using a single-energy value. Low-energy values, from 70 to 90 kV, increase iodine contrast [44]. These values improve the contrast-to-noise ratio in children who receive small contrast volumes at slow injection rates and increase the detection of subtle contrast enhancement. Conversely, high-energy values, from 100 to 150 kV, decrease iodine contrast. These values reduce metal and beam-hardening artifacts from injected CM in the subclavian vein, axillary vein, or superior vena cava [45, 46].

Scan thickness

Scan thickness should be the thinnest possible, because thinner slices improve contrast-to-noise ratio and, consequently, image quality. For this reason, slice thickness should be 0.6 mm and increment 0.4 mm. However, when is necessary evaluate larger structures or for quantification of ventricular function, slice thickness of 1.2 mm should be used to reduce mA and, consequently, radiation dose [47, 48].

Image reconstruction

Image reconstruction is based on an iterative reconstruction algorithm that employs measured raw and simulated data to generate image estimates that are compared and corrected in cycles at different strength levels. Iterative reconstruction techniques provide similar image quality to filtered back-projection with lower tube voltage reducing radiation exposure. Iterative reconstruction techniques decrease artifacts associated with filtered back-projection, such as blooming and beam-hardening artifacts. Medium smooth convolution kernel should be used with a low-intermediate strength [49].

Post-processing

For extra-cardiac structures evaluation are necessary Multi Planar Reformations in sagittal and coronal planes. For coronary arteries are necessary Curved Planar Reformations to display their origin and course. For cardiac structures with prospective or retrospective ECG-gated acquisition, the best cardiac phase with minimal cardiac motion should be manually selected. Sometimes, could be necessary to reconstruct several phases to determine the best frame of cardiac rest. In case of irregular heart rate, it might be advisable to reconstruct phases according to milliseconds rather than relative percentage intervals because this method could be superior. Maximum Intensity Projection images are necessary for vascular structures. Volume Rendering Reconstructions are necessary for a tridimensional overview of cardiac and great vessel anatomy [50, 51].

Radiation dose

Radiation dose reduction in pediatric patient is important because organ sensitivity to radiation is much higher than in adults, and a risk of developing cancer in the future cannot be totally ruled out. All CT examinations should employ a low-dose protocol, including weight-adapted settings with an automatic modulation of tube current. Third-generation DSCT allows dose saving, reducing the energy of the X-ray beam from 80 to 70 kV [52, 53]. Moreover, prospective ECG-triggered high-pitch spiral scan mode allows minimal

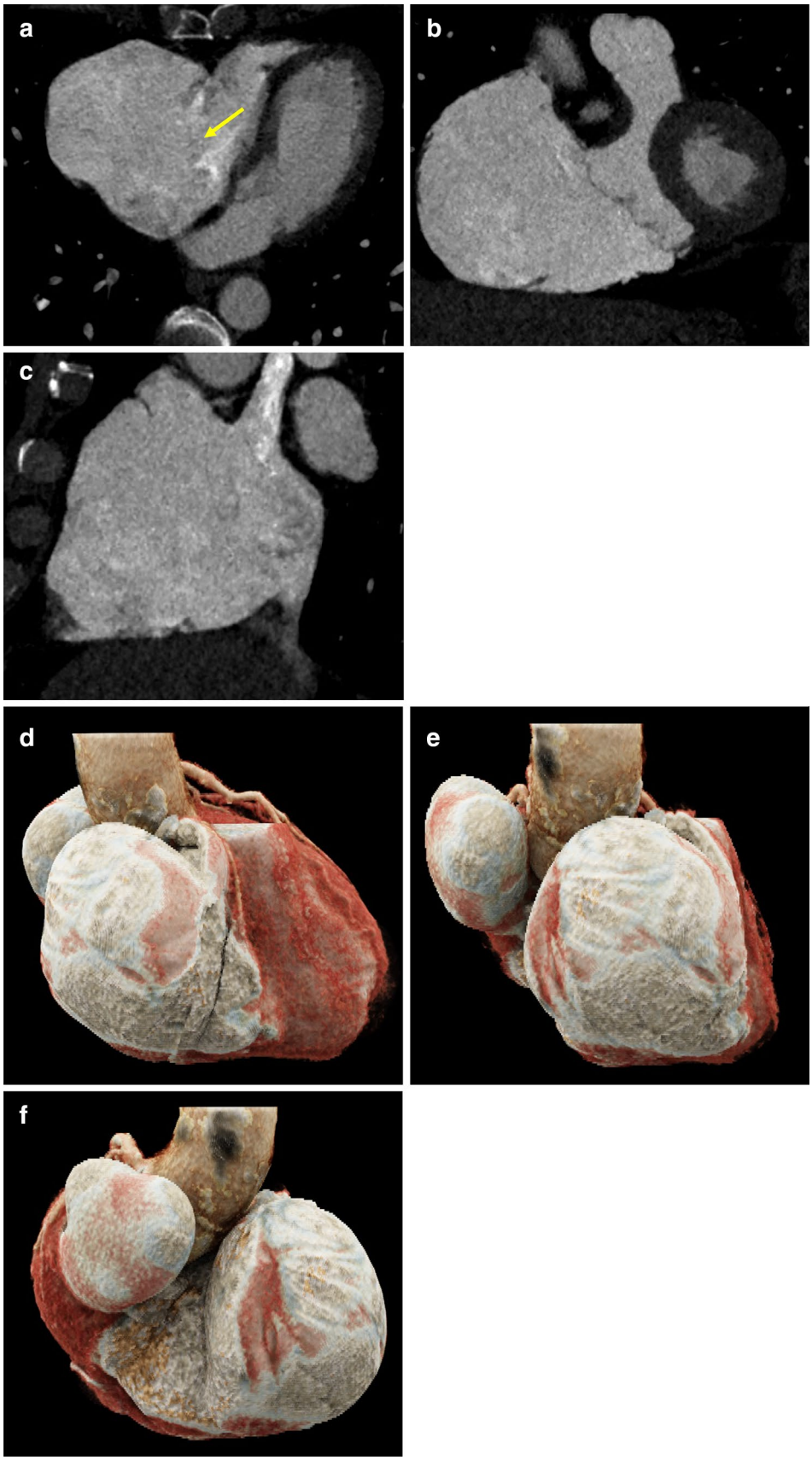

Fig. 3 DSCT images in a 5-year-old patient with Ebstein anomaly. Apical and anterior displacement of the tricuspid valve functional orifice (**a**) (yellow arrow). Tricuspid valve regurgitation decrease forward flow across the pulmonary valve reducing systemic cardiac output (**b**) and increase right atrial dimensions (**c**). Volume rendering reconstructions in posterior (**d**), right (**e**) and left (**f**) views

Table 5 DSCT protocol in a 5-year-old patient with Ebstein anomaly

Scan parameters	
Tube voltage	70 kV
Tube current	60–90 mAs
Pitch factor	3.2
Collimation	2 × 196 × 0.6 mm
Rotation time	0.25 s
Scan protocol	Prospective ECG-triggered high pitch
Reconstruction parameters	
Slice width	0.6 mm
Slice increment	0.4 mm
Kernel–strength	Bv40–3
Cardiac phase	30%
Radiation dose	
CTDI	1.4 mGy
DLP	59.2 mGy * cm
SSDE	0.9 mGy
Effective dose	1.2 mSv
Contrast medium	
Concentration	320 mgI/ml
Dose	0.8 ml/kg
Volume	40 ml

DSCT, electrocardiogram; Bv, Body vascular; $CTDI_{vol}$, volume computed tomography dose index; DLP, dose length product; SSDE, size-specific dose estimates

radiation exposure without significant differences in diagnostic confidence. Using this protocol, radiation exposure is estimated to be less than 1 mSv, which is equivalent to the dose delivered by natural radiation over a 6-month period [54]. Prospective ECG-gated sequential scan mode still provides from 1 to 2 mSv. Retrospective ECG-gated scan mode provides from 2 to 4 mSv [55, 56].

Concerning DECT in the pediatric population, in the few prior publications, the radiation exposure level from DECT is equivalent to or even less than that of a comparable single-energy examination [57]. The optimization of scanner technology, including better iterative reconstruction techniques, improved detector efficiency, and the addition of spectral filtration that attenuates photons in the higher-energy tube. Moreover, DECT scanners can generate virtual non-enhanced images, which have the potential to reduce radiation exposure by eliminating the need for a true non-enhanced acquisition [58, 59].

Case examples

Clinical indications for cardiac CT in the pediatric population with CHDs cover a wide spectrum. Some case examples are provided, all acquired on a DSCT scanner with DE technology (SOMATOM Force, Siemens Heathineers, Forchleim, Germany).

Hypoplastic left heart syndrome

Hypoplastic left heart syndrome (HLHS) comprises a wide spectrum of cardiac malformations, including hypoplasia or atresia of the aortic and mitral valves and hypoplasia of the left ventricle and ascending aorta. The great vessels are normally related in HLHS. HLHS is the fourth most common cardiac malformation to manifest in the first year of life behind ventricular septal defect, transposition of the great arteries, and tetralogy of Fallot. HLHS has a reported prevalence of 0.2 per 1000 live births. Left untreated, HLHS is invariably lethal and is responsible for 25% of early cardiac deaths in neonates. However, the recent evolution of palliative surgical procedures has increased the survival rate in children with these malformations [60].

CT has become a valuable modality in evaluating the complex anatomic findings associated with HLHS. CT provides information for surgical planning, include location and size of the hypoplastic ascending aorta, and post-surgical assessment, such as the modified Fontan procedure, a lateral tunnel created within or near the right atrium to direct blood from the inferior vena cava to the right pulmonary artery to reduce patient cyanosis [61]. A case example of DSCT examination of a 3-year-old patient with HLHS treated with modified Fontan procedure is shown in Fig. 1. CT protocol and radiation dose are summarized in Table 3.

Interrupted aortic arch with patent ductus arteriosus

Interrupted aortic arch (IAA) accounts for approximately 1.5% of all CHDs and 15% of IAA patients have DiGeorge syndrome. The anatomical spectrum varies from an extreme form of aortic coarctation to an absence of an arch segment. According to the site of interruption, three different types are described: type A (30%), the interruption is distal to the origin of left subclavian artery; type B (43%), the interruption is between the left carotid and left subclavian arteries and DiGeorge syndrome is reported in about 50% of patients; type C (17%), the interruption is between the innominate and left carotid arteries. A patent ductus arteriosus (PDA) is invariably present with IAA, and the descending aorta is a continuation of the ductus. Bicuspid aortic valve occurs in 60% of all cases, sub-aortic stenosis occurs in about 20%, and truncus arteriosus in about 10% [62].

CT has become a valuable modality in evaluating the complex anatomic findings associated with IAA. CT can be used to evaluate the type and the level of IAA, the PDA, the aortic valve and potential post-surgical complications [63]. A case example of DSCT examination of a 12-day-old

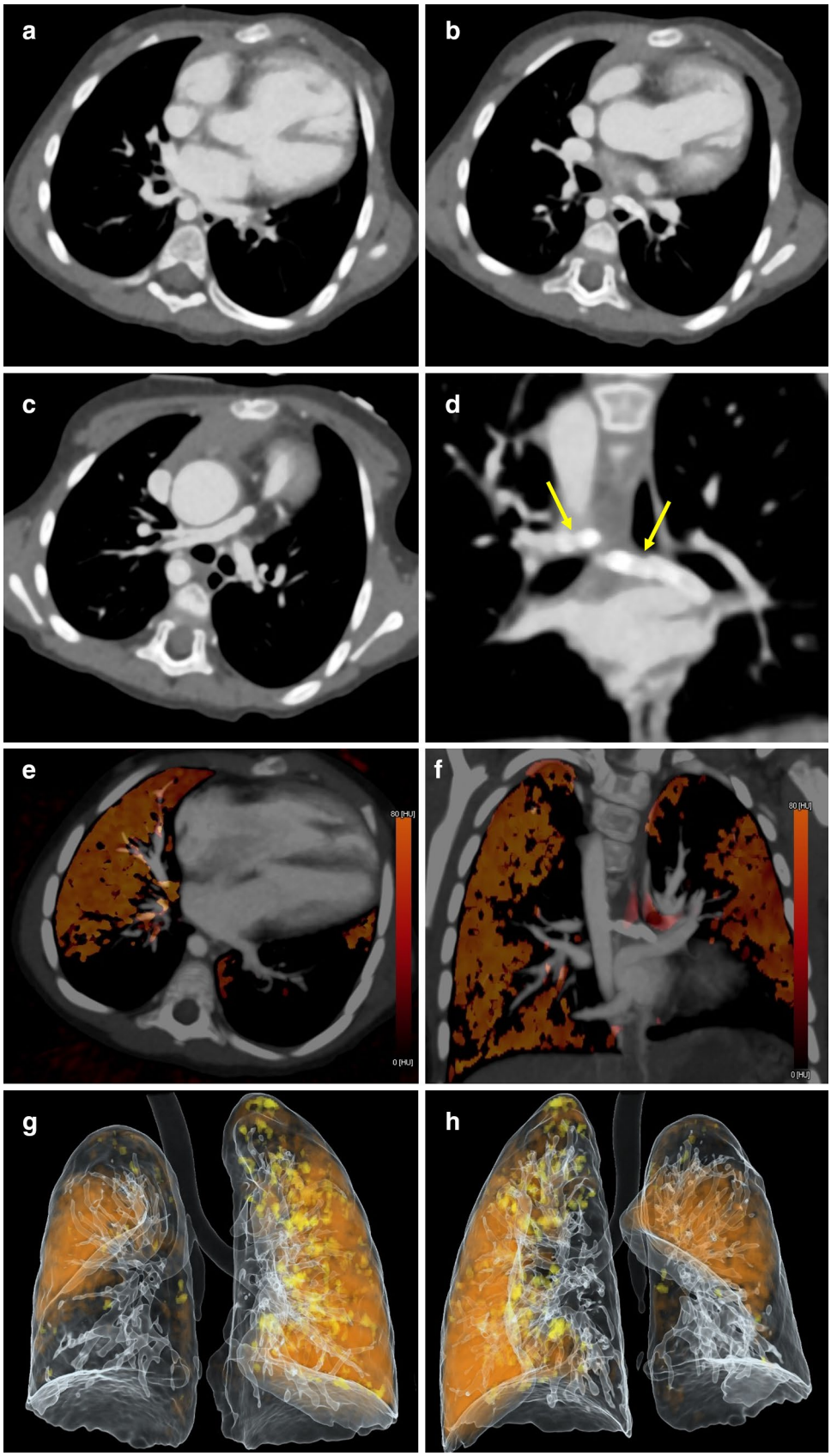

Fig. 4 DSCT images and DE application in a 10-month-old patient with TOF. Large ventricular septum defect (**a**), anterior shift of the aorta over the ventricular septum defect (**b**), right ventricular outflow tract obstruction with pulmonary artery atresia and dextro-position of the aortic arch (**c**). Patency of surgical palliative shunt placement (**d**) (yellow arrows). DE application allows to evaluate the reduction in blood perfusion of the lower lobe of the left lung lower in axial (**e**), and coronal (**f**) views and with volume rendering reconstructions in posterior (**g**) and anterior (**h**) views

Table 6 DSCT protocol and DE application in a 10-month-old patient with TOF

Scan parameters	
Tube voltage (dual energy)	70–150 kV
Tube current	30–60 mAs
Pitch factor	0.2
Collimation	2 × 196 × 0.6 mm
Rotation time	0.25 s
Scan Protocol	Retrospective ECG-gated
Reconstruction parameters	
Slice width	0.6 mm
Slice increment	0.4 mm
Kernel–strength	Bv40–3
Cardiac phase	30%
Radiation dose	
CTDI	0.7 mGy
DLP	23.8 mGy * cm
SSDE	0.7 mGy
Effective dose	1.1 mSv
Contrast medium	
Concentration	320 mgI/ml
Dose	0.5 ml/kg
Volume	4.5 ml

DSCT, electrocardiogram; Bv, Body vascular; $CTDI_{vol}$, volume computed tomography dose index; DLP, dose length product; SSDE, size-specific dose estimates

patient with IAA and PDA is shown in Fig. 2. CT protocol and radiation dose are summarized in Table 4.

Ebstein anomaly

Ebstein anomaly (EA) accounts for < 1% of all CHDs with an equal distribution between male and female. It is a malformation which involves both the tricuspid valve (TV) and the right ventricle (RV). As a consequence of this apical and anterior displacement of the TV functional orifice, functionally RV is variably hypoplastic; the myocardium above the orifice becomes "atrialized" and, thus, thin and dysfunctional; the myocardium below the orifice typically possesses a more normal ventricular wall thickness but is still dysfunctional. The RV impairment and the TV regurgitation decrease forward flow across the pulmonary valve reducing systemic cardiac output and increase right atrial dimensions and pressure thus favoring a right-to-left shunt through the interatrial communication; cyanosis depends upon the right-to-left shunting [64].

CT has become a valuable modality in evaluating the complex anatomic findings associated with EA. CT can be used to evaluate the apical displacement of the TV, RV outflow tract obstruction, intra-cardiac shunts and coronary arteries anomalies. DE technology can be used to evaluate the possible reduction in lung blood volume perfusion [65]. DSCT examination of a 5-year-old patient with EA is shown in Fig. 3. CT protocol and radiation dose are summarized in Table 5.

Tetralogy of Fallot

Tetralogy of Fallot (TOF) occurs in 10% of all CHDs and is the most common cyanotic defect seen in children beyond infancy. It involves the following four anatomic abnormalities of the heart: large ventricle septal defect (VSD), anterior shift of the aorta over the VSD (overriding aorta), RV outflow tract (OT) obstruction, and RV hypertrophy. Within TOF, there is a wide spectrum of presentation: the degree of cyanosis depends on the degree of RVOT obstruction. TOF and pulmonary atresia with VSD occurs in approximately 15–20% of all tetralogy cases and the pulmonary supply is most commonly mediated through a PDA (70%) and less commonly through major aorto-pulmonary collateral arteries (MAPCAs) (30%) [66].

CT has become a valuable modality in evaluating the complex anatomic findings associated with both unrepaired and repaired TOF patients. CT can be used to evaluate the RVOT obstruction, the aortic root anatomy and the overriding aorta, the VSD, the PDA, the MAPCAs, the patency of surgical palliative shunt placement and for long-term sequelae and complications. DE application can be used to evaluate the possible reduction in lung blood volume perfusion [67, 68]. DSCT with DE application examination of a 10-month-old patient with TOF is shown in Fig. 4. CT protocol and radiation dose are summarized in Table 6.

Transposition of the great arteries

Transposition of great arteries (TGA) accounts for 2–5% of all CHDs with a prevalence of about 0.2–0.3 of 1000 births; it is more common in males than in females with a ratio of 2–3:1. It derives from truncal ridge and infundibulum normal spiraling rotation failure during fetal life which results in discordant ventriculo-arterial connection: aorta arises from the morphologically right ventricle (RV) and is located anteriorly and to the right of pulmonary artery (PA) (D-transposition), whereas the PA arises from morphologically left ventricle (LV). This hemodynamic condition is incompatible with life unless a communication exists between the two circulations, which allows a mixing between oxygenated and deoxygenated blood. During neonatal period, patent ductus arteriosus (PDA) and mainly patent foramen ovale (PFO) usually maintain an adequate mixing because they ensure the effective systemic/pulmonary blood flow going, respectively, into the aorta and the PA; as the PDA starts to close and PFO by itself is restrictive in size, infant develops severe cyanosis [69].

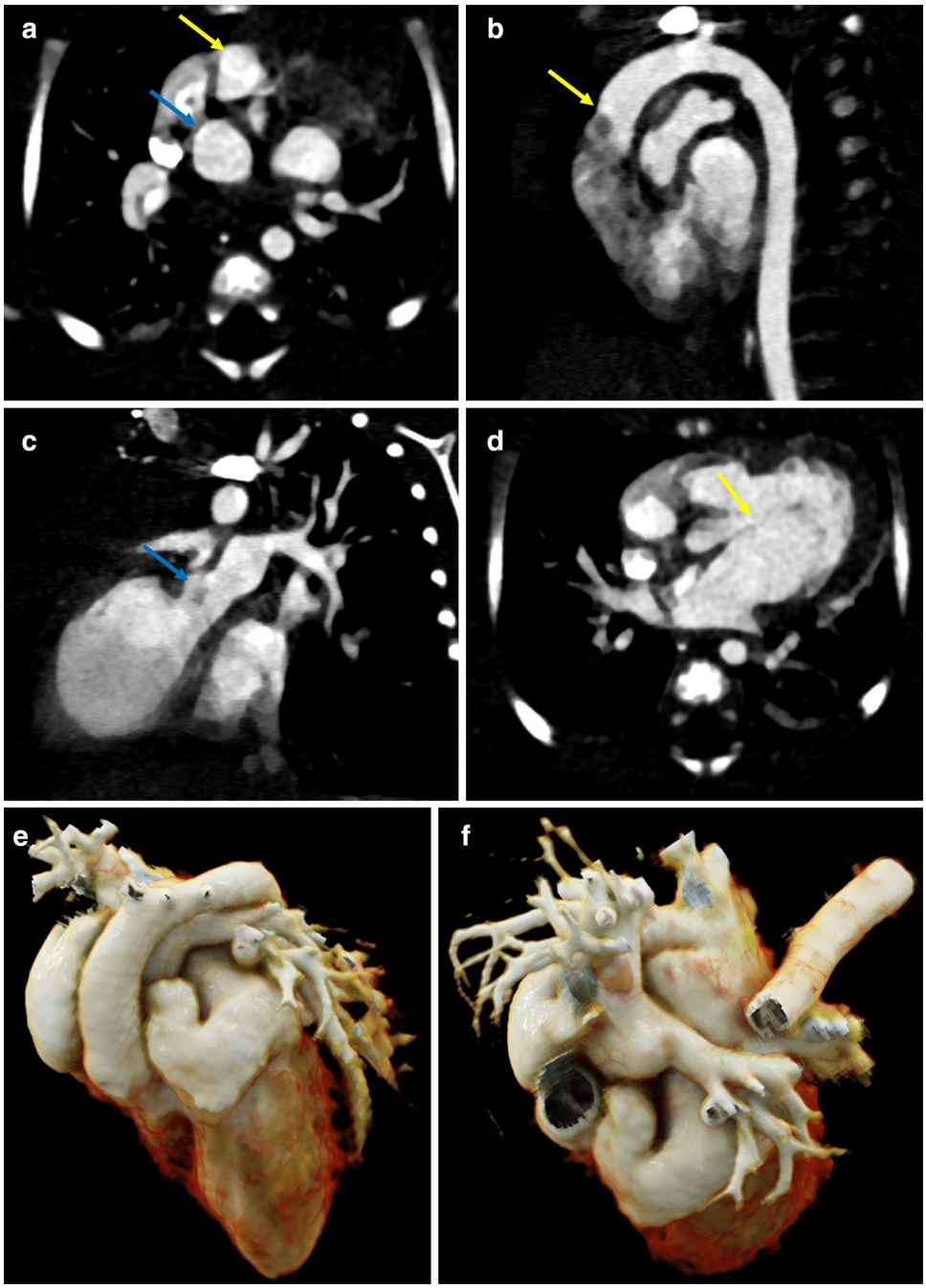

Fig. 5 DSCT images in a 3-day-old patient with TGA. Aorta (yellow arrow) arises from the morphologically right ventricle and is located anteriorly of pulmonary artery (blue arrow) (**a**, **b**). Pulmonary artery (blue arrow) arises from morphologically left ventricle (**a**, **c**). Presence of large ventricular septum defect (**d**) (yellow arrow). Volume rendering reconstructions in superior view with (**e**) and without aorta (**f**)

CT has become a valuable modality in evaluating the complex anatomic findings associated TGA. CT can be used to evaluate the origin and course of the great arteries, the presence and size of the PDA and/or PFO, and any associated anomalies such as LVOT obstruction and aortic coarctation [70]. DSCT examination of a 3-day-old patient with TGA is shown in Fig. 5. CT protocol and radiation dose are summarized in Table 7.

Conclusion

DSCT with DE technology is an important low-invasive diagnostic tool for the evaluation of CHD in pediatric patients, providing relevant information for optimal surgical management. The main drawback of CT, especially in the pediatric population, is the cumulative radiation dose from repeat examinations pre- and post-surgery or endovascular treatment. However, with the introduction of the third-generation DSCT and the use of prospective ECG-triggered high-pitch spiral scan, low tube voltage and tube current and new

Table 7 DSCT protocol in a 3-day-old patient with TGA

Scan parameters	
Tube voltage	70 kV
Tube current	30–60 mAs
Pitch factor	3.2
Collimation	2×196×0.6 mm
Rotation time	0.25 s
Scan protocol	Prospective ECG-triggered high pitch
Reconstruction parameters	
Slice width	0.6 mm
Slice increment	0.4 mm
Kernel–strength	Bv40–3
Cardiac phase	30%
Radiation dose	
CTDI	0.2 mGy
DLP	6.5 mGy*cm
SSDE	0.2 mGy
Effective dose	0.5 mSv
Contrast medium	
Concentration	320 mgI/ml
Dose	0.5 ml/kg
Volume	1.5 ml

DSCT, electrocardiogram; Bv, Body vascular; $CTDI_{vol}$, volume computed tomography dose index; DLP, dose length product; SSDE, size-specific dose estimates

iterative reconstruction algorithms the radiation dose may even be lowered to 1 mSv. Moreover, the speed of scanning reduces any motion-related artifact. Finally, DE technology has the ability to differentiate materials with different atomic numbers with important clinical applications, such as better evaluation of vascular structures and shunts, assessment of the myocardial and lung perfusion and reduction in metal artifact.

For all these reasons, DSCT with DE technology will result in widespread adoption, into clinical practice, for CHDs assessment in pediatric population.

Funding This research did not receive any specific grant from funding agencies in the public, commercial, or not-for-profit sectors.

Compliance with ethical standards

Conflict of interest The authors declared no potential conflicts of interests associated with this study.

Ethical standards All procedures performed in studies involving human participants were in accordance with the ethical standards of the institutional and/or national research committee and with the 1964 Helsinki declaration and its later amendments or comparable ethical standards. Informed consent was obtained from all individual participants included in the study.

References

1. Sun R, Liu M, Lu L, Zheng Y, Zhang P (2015) Congenital heart disease: causes, diagnosis, symptoms, and treatments. Cell Biochem Biophys 72(3):857–860
2. Long CM, Long SS, Johnson PT, Mahesh M, Fishman EK, Zimmerman SL (2015) Utility of low-dose high-pitch scanning for pediatric cardiac computed tomographic imaging. J Thorac Imaging 30(4):W36–W40
3. Booij R, Dijkshoorn ML, van Straten M (2016) Cardiovascular imaging in pediatric patients using dual source CT. J Cardiovasc Comput Tomogr 10:13–21
4. Abbara S, Blanke P, Maroules CD (2016) SCCT guidelines for the performance and acquisition of coronary computed tomographic angiography: a report of the Society of Cardiovascular Computed Tomography Guidelines Committee: endorsed by the North American Society for Cardiovascular Imaging (NASCI). J Cardiovasc Comput Tomogr 10:435–449
5. Johnson JN, Hornik CP, Li JS, Benjamin DK Jr, Yoshizumi TT, Reiman RE, Frush DP, Hill KD (2014) Cumulative radiation exposure and cancer risk estimation in children with heart disease. Circulation 130:161–167
6. Goo HW, Goo JM (2017) Dual-energy CT: new horizon in medical imaging. Korean J Radiol 18(4):555–569
7. McCollough CH, Leng S, Yu L, Fletcher JG (2015) Dual- and multi-energy CT: principles, technical approaches, and clinical applications. Radiology 276(3):637–653
8. Patino M, Prochowski A, Agrawal MD, Simeone FJ, Gupta R, Hahn PF, Sahani DV (2016) Material separation using dual-energy CT: current and emerging applications. RadioGraphics 36(4):1087–1105
9. Siegel MJ, Kaza RK, Bolus DN, Boll DT, Rofsky NM, De Cecco CN, Foley WD, Morgan DE, Schoepf UJ, Sahani DV, Shuman WP, Vrtiska TJ, Yeh BM, Berland LL (2016) White paper of the Society of Computed Body Tomography and Magnetic Resonance on dual-energy CT. Part 1: technology and terminology. J Comput Assist Tomogr 40(6):841–845
10. Foley WD, Shuman WP, Siegel MJ, Sahani DV, Boll DT, Bolus DN, De Cecco CN, Kaza RK, Morgan DE, Schoepf UJ, Vrtiska TJ, Yeh BM, Berland LL (2016) White paper of the Society of Computed Body Tomography and Magnetic Resonance on Dual-Energy CT, part 2: radiation dose and iodine sensitivity. J Comput Assist Tomogr 40(6):846–850
11. De Cecco CN, Schoepf UJ, Steinbach L, Boll DT, Foley WD, Kaza RK, Bolus DN, Morgan DE, Sahani DV, Shuman WP, Siegel MJ, Vrtiska TJ, Yeh BM, Berland LL (2017) White paper of the Society of Computed Body Tomography and Magnetic Resonance on Dual-Energy CT, part 3: vascular, cardiac, pulmonary, and musculoskeletal applications. J Comput Assist Tomogr 41(1):1–7
12. Zhao Y, Wu Y, Zuo Z, Cheng S (2017) CT angiography of the kidney using routine CT and the latest Gemstone Spectral Imaging combination of different noise indexes: image quality and radiation dose. Radiol Med 122(5):327–336
13. Rassouli N, Etesami M, Dhanantwari A, Rajiah P (2017) Detector-based spectral CT with a novel dual-layer technology: principles and applications. Insights Imaging 8(6):589–598
14. Almeida IP, Schyns LE, Öllers MC, van Elmpt W, Parodi K, Landry G, Verhaegen F (2017) Dual-energy CT quantitative imaging: a comparison study between twin-beam and dual-source CT scanners. Med Phys 44(1):171–179
15. Euler A, Obmann MM, Szucs-Farkas Z, Mileto A, Zaehringer C, Falkowski AL, Winkel DJ, Marin D, Stieltjes B, Krauss B, Schindera ST (2018) Comparison of image quality and radiation dose

between split-filter dual-energy images and single-energy images in single-source abdominal CT. Eur Radiol 28(8):3405–3412
16. Martine RJ, Santangelo T, Colas L, Jean-Baptiste F, Duhamel A, Deschildre A, Remy J (2017) Radiation dose levels in pediatric chest CT: experience in 499 children evaluated with dual-source single-energy CT. Pediatr Radiol 47(2):161–168
17. Li M, Zhang GM, Zhao JS, Jiang ZW, Peng ZH, Jin ZT, Sun G (2014) Diagnostic performance of dual-source CT coronary angiography with and without heart rate control: systematic review and meta-analysis. Clin Radiol 69(2):163–171
18. Han BK, Overman DM, Grant K (2013) Non-sedated, free breathing cardiac CT for evaluation of complex congenital heart disease in neonates. J Cardiovasc Comput Tomogr 7:354–360
19. Tucker EW, Jain SK, Mahesh M (2017) Balancing the risks of radiation and anesthesia in pediatric patients. J Am Coll Radiol 14(11):1459–1461
20. Kino A, Zucker EJ, Honkanen A, Kneebone J, Wang J, Chan F, Newman B (2019) Ultrafast pediatric chest computed tomography: comparison of free-breathing versus breath-hold imaging with and without anesthesia in young children. Pediatr Radiol 49(3):301–307
21. Leipsic J, Abbara S, Achenbach S (2014) SCCT guidelines for the interpretation and reporting of coronary CT angiography: a report of the Society of Cardiovascular Computed Tomography Guidelines Committee. J Cardiovasc Comput Tomogr 8:342–358
22. Meyer M, Haubenreisser H, Schoepf UJ, Vliegenthart R, Leidecker C, Allmendinger T, Lehmann R, Sudarski S, Borggrefe M, Schoenberg SO, Henzler T (2014) Closing in on the K edge: coronary CT angiography at 100, 80, and 70 kV-initial comparison of a second- versus a third-generation dual-source CT system. Radiology 273:373–382
23. Fleischmann U, Pietsch H, Korporaal JG, Flohr TG, Uder M, Jost G, Lell MM (2018) Impact of contrast media concentration on low-kilovolt computed tomography angiography: a systematic preclinical approach. Invest Radiol 53(5):264–270
24. Saake M, Lell MM, Rompel O, Gloeckler M, May M, Eller A, Achenbach S, Uder M, Wuest W (2014) Contrast medium application in pediatric high-pitch cardiovascular CT angiography: manual or power injection? J Cardiovasc Comput Tomogr 8(4):315–322
25. Stenzel F, Rief M, Zimmermann E (2014) Contrast agent bolus tracking with a fixed threshold or a manual fast start for coronary CT angiography. Eur Radiol 24:1229–1238
26. Sorantin E, Weissensteiner S, Hasenburger G, Riccabona M (2013) CT in children–dose protection and general considerations when planning a CT in a child. Eur J Radiol 82:1043–1049
27. Sun K, Liu GR, Li YC, Han RJ, Cui LF, Ma LJ, Li LG, Li CY (2013) Intravenous contrast material administration at high-pitch dual-source CT coronary angiography: bolus-tracking technique with shortened time of respiratory instruction versus test bolus technique. Chin Med Sci J 27(4):225–231
28. Gao Y, Lu B, Hou Z, Yu F, Cao H, Han L, Wu R (2012) Low dose dual-source CT angiography in infants with complex congenital heart disease: a randomized study. Eur J Radiol 81(7):e789–e795
29. Xie L, Liu Z, Zhang X, Xu K, Xu Q, Lu L, Hu C, Han S, Li J (2018) Electrocardiography-gated dual-source computed tomography in the detection of atrial septal aneurysm. Exp Ther Med 16(5):4260–4264
30. Kanie Y, Sato S, Tada A, Kanazawa S (2017) Image quality of coronary arteries on non-electrocardiography-gated high-pitch dual-source computed tomography in children with congenital heart disease. Pediatr Cardiol 38(7):1393–1399
31. Mueller-Lisse UG, Marwitz L, Tufman A, Huber RM, Zimmermann HA, Walterham A, Wirth S, Paolini M (2018) Less radiation, same quality: contrast-enhanced multi-detector computed tomography investigation of thoracic lymph nodes with one millisievert. Radiol Med 123(11):818–826
32. Li T, Zhao S, Liu J, Yang L, Huang Z, Li J, Luo C, Li X (2017) Feasibility of high-pitch spiral dual-source CT angiography in children with complex congenital heart disease compared to retrospective-gated spiral acquisition. Clin Radiol 72(10):864–870
33. La Grutta L, Marasà M, Toia P, Ajello D, Albano D, Maffei E, Grassedonio E, Novo G, Galia M, Caruso G, Novo S, Cademartiri F, Midiri M (2017) Integrated non-invasive approach to atherosclerosis with cardiac CT and carotid ultrasound in patients with suspected coronary artery disease. Radiol Med 122(1):16–21
34. Ippolito D, Fior D, Franzesi CT, Riva A, Casiraghi A, Sironi S (2017) Diagnostic accuracy of 256-row multidetector CT coronary angiography with prospective ECG-gating combined with fourth-generation iterative reconstruction algorithm in the assessment of coronary artery bypass: evaluation of dose reduction and image quality. Radiol Med 122(12):893–901
35. Koplay M, Kizilca O, Cimen D, Sivri M, Erdogan H, Guvenc O, Oc M, Oran B (2016) Prospective ECG-gated high-pitch dual-source cardiac CT angiography in the diagnosis of congenital cardiovascular abnormalities: radiation dose and diagnostic efficacy in a pediatric population. Diagn Interv Imaging 97(11):1141–1150
36. Messerli M, Dewes P, Scholtz JE, Arendt C, Wildermuth S, Vogl TJ, Bauer RW (2016) Evaluation of an adaptive detector collimation for prospectively ECG-triggered coronary CT angiography with third-generation dual-source CT. Eur Radiol 28(5):2143–2150
37. Cesare E, Patriarca L, Panebianco L, Bruno F, Palumbo P, Cannizzaro E, Splendiani A, Barile A, Masciocchi C (2018) Coronary computed tomography angiography in the evaluation of intermediate risk asymptomatic individuals. Radiol Med 123(9):686–694
38. Alis J, Latson LA Jr, Haramati LB, Shmukler A (2018) Navigating the pulmonary perfusion map: dual-energy computed tomography in acute pulmonary embolism. J Comput Assist Tomogr 42(6):840–849
39. Hwang HJ, Hoffman EA, Lee CH (2017) The role of dual-energy computed tomography in the assessment of pulmonary function. Eur J Radiol 86:320–334
40. Rizzo S, Femia M, Radice D, Del Grande M, Franchi D, Origgi D, Buscarino V, Mauro A, Bellomi M (2018) Evaluation of deep myometrial invasion in endometrial cancer patients: is dual-energy CT an option? Radiol Med 123(1):13–19
41. Otrakji A, Digumarthy SR, Lo Gullo R, Flores EJ, Shepard JA, Kalra MK (2016) Dual-energy CT: spectrum of thoracic abnormalities. RadioGraphics 36(1):38–52
42. Hachulla AL, Lador F, Soccal PM, Montet X, Beghetti M (2016) Dual-energy computed tomographic imaging of pulmonary hypertension. Swiss Med Wkly 146:w14328
43. Magarelli N, De Santis V, Marziali G, Menghi A, Burrofato A, Pedone L, Del Prete D, Iezzi R, de Waure C, D'andrea M, Leone A, Colosimo C (2018) Application and advantages of monoenergetic reconstruction images for the reduction of metallic artifacts using dual-energy CT in knee and hip prostheses. Radiol Med 123(8):593–600
44. Muto M, Giurazza F, Ambrosanio G, Vassallo P, Briganti F, Tecame M, Schena E, De Nicola M, Sgreccia A, Giannoni M, Peschillo S, Diana F, Guidetti G, Guarnieri G (2017) Stent-assisted coiling in ruptured cerebral aneurysms: multi-center experience in acute phase. Radiol Med 122(1):43–52
45. Niola R, Giurazza F, Torbica A, Schena E, Silvestre M, Maglione F (2017) Predelivery uterine arteries embolization in patients with placental implant anomalies: a cost-effective procedure. Radiol Med 122(1):77–79
46. Paolicchi F, Bastiani L, Guido D, Dore A, Aringhieri G, Caramella D (2018) Radiation dose exposure in patients affected by

lymphoma undergoing repeat CT examinations: how to manage the radiation dose variability. Radiol Med 123(3):191–201
47. Compagnone G, Padovani R, D'Avanzo MA, Grande S, Campanella F, Rosi A, Italian Working Group on Interventional Radiology (2018) Summary of the Italian inter-society recommendations for radiation protection optimization in interventional radiology. Radiol Med 123(5):378–384
48. Marukawa Y, Sato S, Tanaka T, Tada A, Kanie Y, Kanazawa S (2017) Evaluating low-kV dual-source CT angiography by high-pitch spiral acquisition and iterative reconstruction in pediatric congenital heart disease patients. Acta Med Okayama 71(5):407–412
49. Sun J, Zhang Q, Duan X, Zhang C, Wang P, Jia C, Liu Y, Peng Y (2018) Application of a full model-based iterative reconstruction (MBIR) in 80 kVp ultra-low-dose paranasal sinus CT imaging of pediatric patients. Radiol Med 123(2):117–124
50. Qin L, Ma Z, Yan F, Yang W (2018) Iterative model reconstruction (IMR) algorithm for reduced radiation dose renal artery CT angiography with different tube voltage protocols. Radiol Med 123(2):83–90
51. Chen B, Zhao S, Gao Y, Cheng Z, Duan Y, Das P, Wang X (2019) Image quality and radiation dose of two prospective ECG-triggered protocols using 128-slice dual-source CT angiography in infants with congenital heart disease. Int J Cardiovasc Imaging 35(5):937–945
52. Tomà P, Cannatà V, Genovese E, Magistrelli A, Granata C (2017) Radiation exposure in diagnostic imaging: wisdom and prudence, but still a lot to understand. Radiol Med 122(3):215–220
53. Kim JS, Kwon SM, Kim JM, Yoon SW (2017) New organ-based tube current modulation method to reduce the radiation dose during computed tomography of the head: evaluation of image quality and radiation dose to the eyes in the phantom study. Radiol Med 122(8):601–608
54. Ruffino MA, Fronda M, Discalzi A, Isoardi P, Bergamasco L, Ropolo R, Righi D, Fonio P (2018) Radiation dose during endovascular aneurysm repair (EVAR): upgrade of an angiographic system from standard to Eco mode. Radiol Med 123(12):966–972
55. Nardi C, Salerno S, Molteni R, Occhipinti M, Grazzini G, Norberti N, Cordopatri C, Colagrande S (2018) Radiation dose in non-dental cone beam CT applications: a systematic review. Radiol Med 123(10):765–777
56. Siegel MJ, Curtis WA, Ramirez-Giraldo JC (2016) Effects of dual-energy technique on radiation exposure and image quality in pediatric body CT. AJR Am J Roentgenol 207(4):826–835
57. Weinman JP, Mirksy DV, Jensen AM, Stence NV (2019) Dual energy head CT to maintain image quality while reducing dose in pediatric patients. Clin Imaging 93:83–86
58. Agliata G, Schicchi N, Agostini A, Fogante M, Mari A, Maggi S, Giovagnoni A (2019) Radiation exposure related to cardiovascular CT examination: comparison between conventional 64-MDCT and third-generation dual-source MDCT. Radiol Med 124(8):753–761
59. Riccardi L, De Monte F, Cretti F, Pini S, Zucca S, Quattrocchi MG, Origgi D, Del Vecchio A, Giordano C, Marini P, Lisciandro F, Trevisiol E, Zefiro D, Cutaia C, D'Ercole L, Gabusi M, Scaggion A, Paiusco M (2018) Use of radiation dose index monitoring software in a multicenter environment for CT dose optimization. Radiol Med 123(12):944–951
60. Cheasty E, Mahboobani S, Rubens M, Nicol E (2018) The use of cardiovascular CT for the follow up of paediatric hypoplastic left heart syndrome. J Cardiovasc Comput Tomogr. https://doi.org/10.1016/j.jcct.2018.10.021
61. Goo HW (2017) Serial changes in anatomy and ventricular function on dual-source cardiac computed tomography after the Norwood procedure for hypoplastic left heart syndrome. Pediatr Radiol 47(13):1776–1786
62. Hanneman K, Newman B, Chan F (2017) Congenital variants and anomalies of the aortic arch. Radiographics 37(1):32–51
63. Goudar SP, Shah SS, Shirali GS (2016) Echocardiography of coarctation of the aorta, aortic arch hypoplasia, and arch interruption: strategies for evaluation of the aortic arch. Cardiol Young 26(8):1553–1562
64. Yuan SM (2017) Ebstein's anomaly: genetics, clinical manifestations, and management. Pediatr Neonatol 58(3):211–215
65. Silva GVRD, Miana LA, Caneo LF, Turquetto ALR, Tanamati C, Penha JG, Jatene FB, Jatene MB (2019) Early and long-term outcomes of surgical treatment of Ebstein's anomaly. Braz J Cardiovasc Surg. https://doi.org/10.21470/1678-9741-2018-0333
66. Goo HW (2018) Coronary artery anomalies on preoperative cardiac CT in children with tetralogy of Fallot or Fallot type of double outlet right ventricle: comparison with surgical findings. Int J Cardiovasc Imaging 34(12):1997–2009
67. Barbiero G, Groff S, Battistel M, Casarin A, Guarise A, Miotto D (2018) Are iatrogenic renal artery pseudoaneurysms more challenging to embolize when associated with an arteriovenous fistula? Radiol Med 123(10):742–752
68. Lapierre C, Dubois J, Rypens F, Raboisson MJ, Déry J (2016) Tetralogy of Fallot: preoperative assessment with MR and CT imaging. Diagn Interv Imaging 97(5):531–541
69. Leone MB, Giannotta M, Palazzini M, Cefarelli M, Martìn Suàrez S, Gotti E, Bacchi Reggiani ML, Zompatori M, Galiè N (2017) A new CT-score as index of hemodynamic changes in patients with chronic thromboembolic pulmonary hypertension. Radiol Med 122(7):495–504
70. Odawara Y, Kawamura N, Yamasaki Y, Hashimoto J, Ishikawa S, Honda H (2019) Evaluation of coronary artery variations using dual-source coronary computed tomography angiography in neonates with transposition of the great arteries. Jpn J Radiol 37(4):308–314